Hydrophobically Modified Dendrimers as Inverse Micelles: Formation of Cylindrical Multidendrimer Nanostructures

Franziska Gröhn, Barry J. Bauer, and Eric J. Amis*

Polymers Division, National Institute of Standards and Technology, Gaithersburg, Maryland 20899

Received October 6, 2000; Revised Manuscript Received May 29, 2001

ABSTRACT: Poly(propyleneimine) dendrimers with stearyl end groups are investigated as inverse micelles in toluene. While the initial dendrimers have a spherical structure with a collapsed core, solubilization of metal salt hydrate leads to the formation of cylindrical multidendrimer structures with swollen, metal-salt-filled dendrimer cores. The cylindrical structure can be deduced from the small-angle neutron (SANS) as well as from the X-ray scattering (SAXS) pair distance distribution function. While the neutron scattering leads to a two-step cross-sectional density profile, the X-ray scattering is sensitive only to the metal-salt-stained core. The gold salt inside the dendrimers was reduced to form colloidal particles, and upon reduction the cylindrical structure breaks up and spherical colloids are formed. The sizes are larger than would be expected if the gold salt loading of one dendrimer formed one particle, indicating that the ions from several dendrimers are combined. These dendrimer-stabilized metal colloids represent hybrid structures that have potential importance as selective catalysts and in the formation of composite materials with special optical properties.

Introduction

High-generation dendrimers in solution can be approximated as homogeneous spheres,[1,2] but there is sufficient space available inside the dendrimer molecules that allows them to act as a "host" for smaller guest molecules. The encapsulation of a guest into a "dendritic box" was first shown by Meijer by the encapsulation of the organic dye molecule Bengal Rose into poly(propyleneimine) (PPI) dendrimers modified with amino acids.[3] The observed "permeability" of dendrimers to small molecules has motivated many further studies and initiated the consideration of a variety of potential applications in areas such as drug delivery, catalysis, and chemical sensors.[4−6]

The "molecular encapsulation" idea has then been applied to different kinds of dendrimers and modified dendrimers in different solvents. Hydrophobically modified PPI dendrimers were shown to trap Bengal Rose in ethanol and not to release it in *n*-hexane solution,[7] while hydrophobically modified poly(amidoamine) dendrimers have been demonstrated to transport copper(II) sulfate from an aqueous solution into an organic phase.[8] Meijer et al. found that the hydrophobically modified PPI dendrimers show a remarkable selectivity in the extraction of solutes of different acidity and hydrophobicity.[9] Further, dendrimers with a fluorinated shell are soluble in supercritical carbon dioxide and can extract an ionic dye from water into the supercritical carbon dioxide.[10] Sulfonate-terminated amphiphilic dendrimers with hydrophobic carbosilane cores demonstrated the ability to enhance the solubility of lipophilic molecules in water.[11] A summary can be found in a recent review.[12] In all of these experiments, the amphiphilic dendrimer acts as a nanoenvironment similar to that encountered in micelles or inverse micelles, solubilizing the guest in a solvent of different polarity. Thus, these modified dendrimers have also been considered "unimolecular micelles".[7,12,13]

Several studies on the binding of the guest to the dendrimer host have been performed by photometric measurements and different kinds of spectroscopy.[14−19] Here, we are interested in characterizing the nanoscale structure of dendrimers that act like inverse micelles. We use dendrimers with a hydrophilic PPI core that have been modified with hydrophobic chains attached to the dendrimer terminal groups. Our choice for this system has been motivated by previous studies regarding the inclusion of dye molecules and by studies on these dendrimers at the air−water interface where they behave as "dendritic surfactants" forming stable monolayers.[20] At the interface, the hydrophobic alkyl chains presumably are aligned perpendicular to the water surface, and the dendritic PPI core faces the aqueous phase. The aggregation of these molecules in water points to the existence of bilayers for which a similar conformation of the dendrimers has been postulated. Very recently, Langmuir−Blodgett films of PPI dendrimers modified with palmitoyl- and azobenzene-containing alkyl chains have allowed the formation of "photoresponsive dendritic monolayers".[21]

In this study, we investigate PPI dendrimers modified with stearyl groups filled a with a gold salt hydrate $HAuCl_4 \cdot 3H_2O$ in toluene solution. The use of the gold salt hydrate not only allows for the addition of a well-defined amount of salt and water but also allows for a study of the structure by scattering techniques. The water provides contrast for a small-angle neutron scattering (SANS) experiment when using deuterated toluene as solvent, and the gold can provide contrast for a complementary small-angle X-ray scattering (SAXS) experiment. Furthermore, the gold salt hydrate can serve as a precursor to investigate whether the hydrophobically modified dendrimers can be used as confined reaction spaces to form noble metal colloids as has been previously observed in inverse micelles.

Experimental Section

Sample Preparation. Fifth-generation (G5) poly(propyleneimine) dendrimers (Astramol)[22] with 64 primary amine groups (DAB-dendr-$(NH_2)_{64}$) modified with octadecanoic acid were provided by DSM.[23,32] Toluene solutions of G5 fatty acid modified dendrimer with a dendrimer mass fraction of 1% were prepared at 55 °C. The desired amount of $HAuCl_4 \cdot 3H_2O$ was

10.1021/ma0017384
Published on Web 09/04/2001

added as solid salt, and the solution was gently stirred at 55 °C, resulting in a clear yellow solution. For SANS experiments, deuterated toluene was used as solvent. Reduction of the gold was performed by addition of a solution of sodium borohydride in diglyme.

Small-Angle Neutron Scattering (SANS). Samples for SANS measurements were transferred into optical quality quartz banjo cells with 1 mm path length. SANS studies were performed at the National Center for Neutron Research at the National Institute of Standards and Technology.[24] Measurements were made using the 30 m SANS instrument with a neutron wavelength $\lambda = 0.6$ nm and wavelength spread of $\Delta\lambda/\lambda = 0.15$. The sample-to-detector distance was 2.0 m. The span of scattering vector magnitudes ($q = (4\pi/\lambda)\sin(\theta)$ and 2θ the scattering angle) was in the range $0.2\ \text{nm}^{-1} < q < 3.2\ \text{nm}^{-1}$. All measurements were performed at 55 °C. Data were corrected for empty quartz cell scattering, electronic background, and detector uniformity and converted to an absolute scale using secondary standards. The data were further corrected by subtracting the contributions from solvent scattering and incoherent background.

Small-Angle X-ray Scattering (SAXS). SAXS data were collected at the Advanced Polymer Beamline at Brookhaven National Laboratory, X27C. The radiation spectrum from the source was monochromated using a double multilayer monochromator and collimated with three 2° tapered tantalum pinholes to give an intense X-ray beam at $\lambda = 1.307$ Å.[25] A 2D image plate detector (BAS2000, Fuji) was used. The sample-to-detector distance was 1.0 m. A vacuum chamber was placed between the sample and detector to reduce air scattering and absorption. The span of scattering vector magnitudes was in the range $0.30\ \text{nm}^{-1} < q < 3.7\ \text{nm}^{-1}$. Scattering patterns from silver behenate and Lupolen were used for angular and absolute intensity scale calibration, respectively. A parallel plate ionizing detector placed before the sample cell was used to record the incident intensities. All measurements were performed at 55 °C.

The experimental intensities were corrected for incident intensity and for background scattering from the camera and empty cell. The correction for pixel-by-pixel detector sensitivity was established from the scattering by an iron(0) source. The two-dimensional data were circularly averaged. Uncertainties were calculated from the standard deviation of the pixel statistics in the averaged annulus. The scattering curves presented here were obtained by further averaging three to four individual measurements. The uncertainties are the standard deviations of the mean intensity and are plotted only when the uncertainty limits are larger than the size of the plotted data points. All scattering intensities were corrected for solvent scattering.

Scattering Data Analysis. After subtraction of incoherent background, the scattering curve $I(q)$ is Fourier transformed into the three-dimensional averaged pair distance distribution function $P(r)$ via the relationship

$$I(q) = 4\pi \int_{r=0}^{\infty} P(r)\,\frac{\sin(qr)}{qr}\,\mathrm{d}r \qquad (1)$$

where r is the radial distance and q is the scattering wave vector magnitude. We apply the indirect transformation method in order to minimize termination effects. We use the program ITP, *Indirect transformation for the calculation of* $P(r)$, by Glatter,[26−28] which includes smoothing of the primary data by a weighted least-squares procedure (estimation of the optimum stabilization parameter based on a stability plot), desmearing, and transforming into real space simultaneously. For the SANS measurements, the actual calculations dealing with the experimental scattering curves accounted for the measured beam profile and the wavelength distribution of the experimental setup. For the SAXS measurements, the wavelength distribution is smaller than 1%, and the beam is focused via a pinhole collimation system to about 100−200 μm diameter. Therefore, smearing effects are not considered in the case of the SAXS data analysis. The pair distance distribution function $P(r)$ is calculated in a model-free way, and thus in the case of a well-defined particle morphology it indicates the geometric features of the scattering system, e.g., spherical, cylindrical, or lamellar symmetry. Once the geometry is identified, alternative equations can be applied; e.g., for cylinders the cross-sectional pair distribution function $P_c(r)$ can be calculated via

$$qI(q) = 2\pi \int_{r=0}^{\infty} P_c(r)\, J_0(qr)\, \mathrm{d}r \qquad (2)$$

where $J_0(x)$ is the zero-order Bessel function and the subscript letter c indicates two-dimensionally averaged quantities.

Radial difference scattering length density (or electron density) profiles $\Delta\rho(x)$ are calculated from the pair distance distribution function $P_c(r)$ by calculation of the convolution square root ("deconvoluting") using the program DECON,[29−31] which applies in the case of cylinders,

$$P_c(r) = r \int_{x=-\infty}^{\infty} \Delta\rho_c(r)\, \Delta\rho_c(x - r)\, \mathrm{d}x \qquad (3)$$

where $\Delta\rho_c(x)$ is the radial scattering length (or electron) density difference between the particle and the surrounding medium. This deconvolution is possible in cases where interparticular contributions are negligible, and the experimental scattering function $I(q)$ is identical with the particle form factor.

Transmission Electron Microscopy (TEM). Carbon-coated copper grids, 300 mesh, were extensively washed in chloroform reflux in order to remove Formvar. Specimens were prepared by depositing the sample solutions on the grid and drying in air at 55 °C. TEM images were obtained at 120 kV with a Phillips 400 T at a magnification of 46 000×.

Results and Discussion

Structure of Inverse Micelles. When stirring solutions of hydrophobically modified poly(propyleneimine) dendrimer over solid $HAuCl_4 \cdot 3H_2O$, the color of the solution turns yellow, indicating the solubilization of the gold salt with the dendrimers. We have prepared samples with an excess of gold salt as well as samples with controlled stoichiometries of gold salt. The maximum amount that is completely dissolved in the toluene solution corresponds to a stoichiometric ratio of gold salt to dendrimer primary amine groups (64 per dendrimer-molecule) of 1:1. In addition, comparison of the absorption of the gold salt in the different solutions by eye reveals an agreement of the saturated and the 1:1 loaded solution. Solutions with loading ratios 1:2, 1:4, and 1:8 show a smaller absorption.

The scattering results from a sample with a maximum load of gold salt, i.e., a molar ratio of 1:1 to dendrimer end groups, are shown in Figure 1. It shows the SANS data for the initial dendrimer and the SANS and SAXS data after solubilization of the gold salt. The initial dendrimer (squares in Figure 1) exhibits a spherical structure. The radius of gyration R_g for the scattering curve shown is $R_g = 2.2$ nm. This is in agreement with previous reports that have studied single-chain form factors of the fatty acid and the dendrimer components of these hydrophobically modified dendrimers[32] and their size in different solvents at different temperatures.[33] The measured size of the dendrimer corresponds to the size of a collapsed dendrimer core plus a fatty acid shell.

The neutron scattering curve for the sample after addition of gold salt hydrate (circles in Figure 1) shows a shift of the first minimum to lower scattering vector magnitudes, q; i.e., the size of the structure increases. This is due to the swelling of the dendrimer upon solubilization of the gold salt hydrate. In addition, the

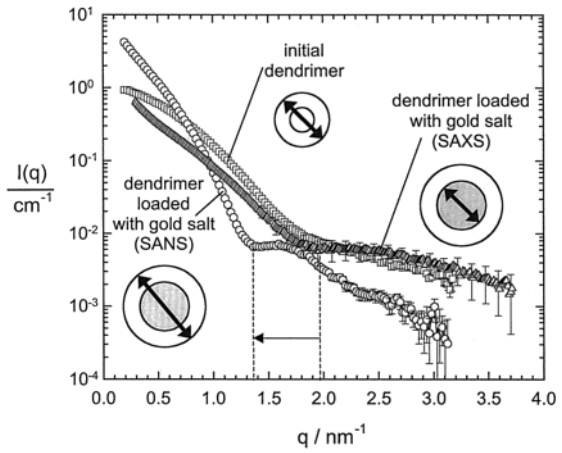

Figure 1. Small-angle neutron scattering curve for the initial G5 poly(propyleneimine) dendrimer in toluene at 55 °C (squares) and small-angle neutron scattering curve (circles) and small-angle X-ray scattering curve (triangles) after solubilization of gold salt. Error bars are the standard deviations of the mean intensity. Cartoons indicate what part of the structure is seen in the scattering experiment.

shape of the scattering curve also changes. We note that in this case the measured q range is not large enough to allow conclusions about particle shape from the scaling behavior in a double-logarithmic plot. To analyze the structure of the gold-filled dendrimers in more detail, we thus Fourier transform the scattering curve $I(q)$ into the pair distance distribution function $P(r)$ according to eq 1. The result is shown in Figure 2b. The $P(r)$ shows a shape typical of a cylindrical structure. The diameter of the cylinder is about 6 nm from the inflection point after the maximum, while the length of the cylinder is about 21 nm from the abscissa intercept. Some further remarks are necessary about the length of the cylindrical structure. The minimum q value measured $q_{min} = 0.196$ nm^{-1} corresponds to a maximum dimension of 16 nm in real space, and the value of 21 nm for the cylinder length therefore has to be considered an extrapolated value. However, the solution of the transformation is stable, and there is a sufficient range of the linear decrease in the $P(r)$ before 16 nm (the error bars of the calculated $P(r)$ do not dramatically increase for higher r values), so that we consider 21 nm a good estimate for the length of the cylinder. Some polydispersity in average length also cannot be excluded. More importantly, the scattering result shows the existence of a cylindrical structure in solution, which has to result from an aggregation of multiple dendrimers, since the length is clearly larger than the diameter of one dendrimer.

Since the scattering data give conclusive evidence of the cylindrical structure, we can now assume cylindrical geometry as input for further calculations. We repeat the Fourier transform of the scattering curve from Figure 2a, this time using the zero-order Bessel function $J_0(qr)$ transformation (eq 2) instead of the $\sin(qr)/(qr)$ transformation used before, and thereby calculate the cross-sectional pair distance distribution function $P_c(r)$ of the cylinder. The result is shown in Figure 3a. This leads to a better estimate of the cylinder diameter, giving 6.4 nm. In addition, the shape of this cross section $P(r)$ roughly indicates a circular cross section. Furthermore, we deconvolute $P_c(r)$ into a radial scattering length density profile of the cylinder (eq 3). First, we allow a multiple step density profile. The resulting

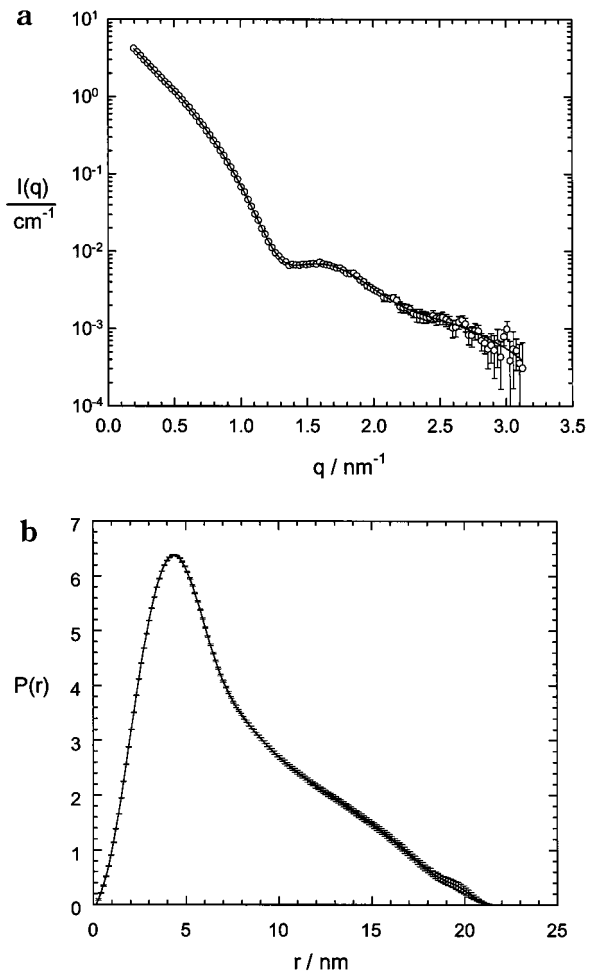

Figure 2. (a) Small-angle neutron scattering curve $I(q)$ for the gold-salt-loaded G5 poly(propyleneimine) dendrimer along with fit to the data. Error bars are the measured standard deviation in $I(q)$. (b) Pair distance distribution function $P(r)$ obtained by indirect Fourier transformation of the scattering data $I(q)$ (program ITP). A cylindrical structure with a diameter of 6 nm and a length of 21 nm becomes evident. Error bars are the standard deviation in the estimation of $P(r)$, which results from the fit to the $I(q)$ data in (a).

radial scattering length profile $\Delta\rho_c(x)$ is shown in Figure 3b as the dotted line. Second, we estimate how many actual steps are present in the density profile from this multiple step profile and the range in which they are located. Then we calculate the radial density profile again, under the assumption of one-step, two-step, and three-step profiles, respectively. We look for the simplest solution that gives the best fit to $P_c(r)$. The result is shown in Figure 3b as the solid line. We find two pronounced steps in the radial density profile: an inner core with a radius of 1.9 nm plus an outer shell of 1.3 nm thickness. The total diameter d is 6.4 nm, as mentioned before. The resolution in real space due to the sampling theorem is expected to be π/q_{max}, i.e., within the range of ± 1 nm.

The measured two-step density profile of the cylinder cross section can be interpreted as a swollen dendrimer core plus a fatty acid shell. The diameter of the "swollen dendrimer" of 3.8 nm is in agreement with previous measurements on G5 poly(propyleneimine) dendrimer (without fatty acid chains attached) in aqueous solution.[34] The thickness of the fatty acid chains is also in agreement with the length of C_{18}-alkyl chains. Since the hydrogen-containing dendrimer is filled with aqueous

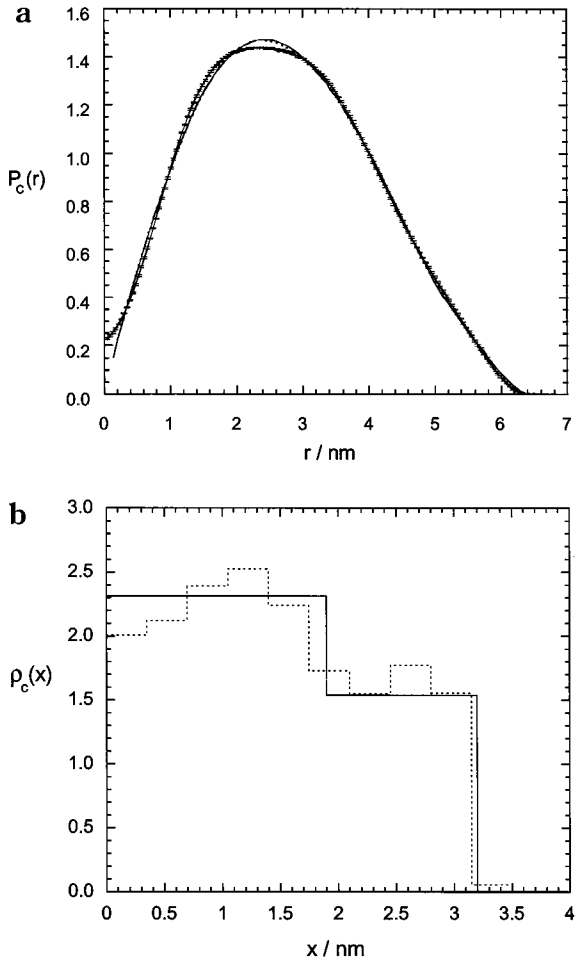

Figure 3. (a) Cross-sectional pair distance distribution function $P_c(r)$ obtained by indirect Fourier transformation of the scattering data $I(q)$ in Figure 2a under assumption of a cylindrical particle geometry (solid line with error bars). Also shown are the fits to these $P_c(r)$ data resulting from the deconvolution for a multistep (dotted line) and a two-step (solid line) radial profile. (b) Radial scattering length density profile $\rho(r)$ obtained by square-root deconvolution of the cross-sectional pair distance distribution function $P_c(r)$ in (a) (program DECON). The dotted line presents the result from the first multistep approximation. The solid line represents the final solution, i.e., the easiest profile corresponding to the best fit to the data: A two step cross-sectional profile becomes evident.

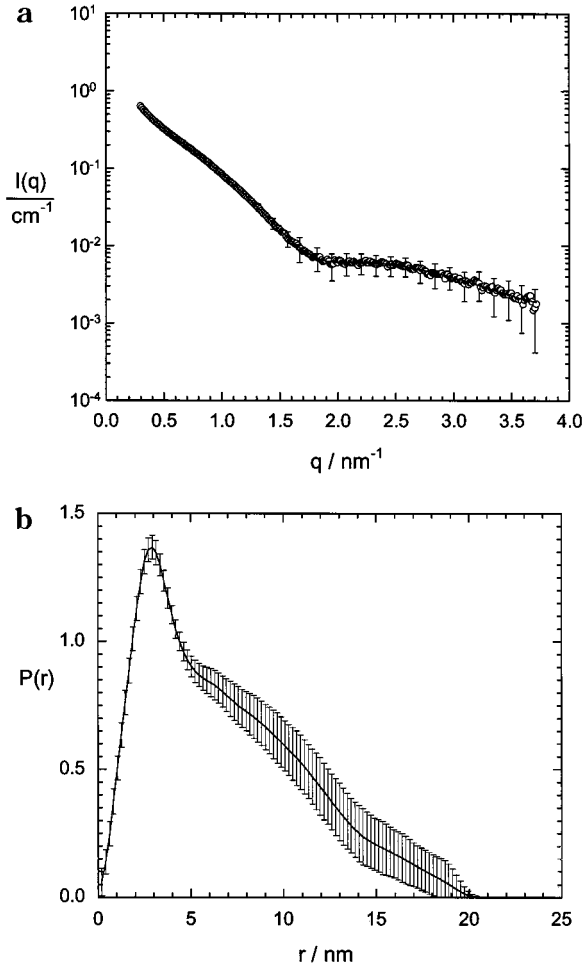

Figure 4. (a) Small-angle X-ray scattering curve $I(q)$ for the gold-salt-loaded G5 poly(propyleneimine) dendrimer along with fit to the data. Error bars are the measured standard deviation in $I(q)$ and plotted for every 10th data point. (c) Pair distance distribution function $P(r)$ obtained by indirect Fourier transformation of the scattering data $I(q)$ (program ITP). A cylindrical structure with a diameter of 4 nm becomes evident. Error bars are the standard deviation in the estimation of $P(r)$, which results from the fit to the $I(q)$ data in (a).

salt hydrate, the contrast of the inner core is higher than the contrast of the outer shell.

To further confirm the structure formed, we have performed small-angle X-ray scattering on the same sample. In the X-ray experiment, only the inner gold-containing core gives contrast, since the electron density difference between the fatty acid chains and the toluene is relatively small. The SAXS data were displayed together with the SANS results in Figure 1 (triangles). The scattering curve and resulting pair distance distribution function are shown in parts a and b of Figure 4, respectively. Again, the $P(r)$ reveals a cylindrical structure. The diameter estimated from the inflection point after the maximum is 4 nm, while the length is 20 nm. The cross-sectional pair distance distribution function $P_c(r)$ in Figure 5 does not intercept the y-axis at the origin, which could be caused by resolution problems below 1 nm.[35] Therefore, we do not deconvolute the SAXS $P_c(r)$ into a radial density profile as was done for the SANS data. However, a diameter of 4 nm is confirmed by the $P_c(r)$ shown in Figure 5. This scale is consistent with the gold-salt-filled inner core of the cylindrical structure, i.e., the first step of the neutron density profile in Figure 3b.

The correspondence of the SAXS and SANS results represents an important confirmation of the deduced cylindrical structure. As pointed out in the experimental part, shape conclusions from the $P(r)$ are possible only for well-defined particle morphologies. Strictly, a $P(r)$ like in Figure 2b—if this was the only result—could be produced by a certain bimodal mixture of small and large particles as was reported for a mixture of small and large lamellae pieces that "simulated" a nearly cylinder-like $P(r)$.[36] However, deconvolution into the density profile indicates that this is not the case here. (While a mixture can produce a $P(r)$ that appears like the one of a cylinder by eye, a deconvolution of such data via eq 2 is usually not possible.) It is not possible to simulate a physically meaningful bimodal distribution to model a combination of $P(r)$ from SANS and SAXS. Figure 6 displays a schematic of the multidendrimer cylindrical structure resulting from the SANS and SAXS data.

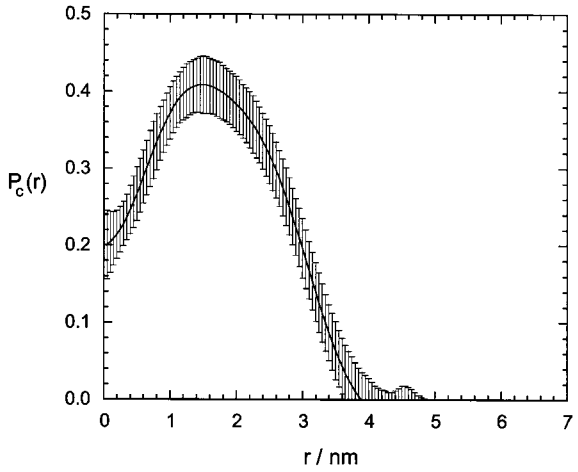

Figure 5. Cross-sectional pair distance distribution function $P_c(r)$ obtained by indirect Fourier transformation of the SAXS data $I(q)$ (Figure 4a) under assumption of a cylindrical particle geometry (program ITP). The $P_c(r)$ function does not intercept the *y*-axis at the origin, which might be due to resolution problems.

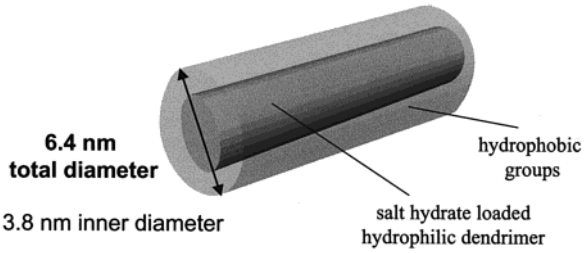

Figure 6. Schematic of the multidendrimer cylindrical structure as deduced from the SAXS and SANS results.

Some comments are necessary on how and why dendrimers can form a cylindrical structure as depicted in Figure 6, in which the individual dendrimer molecules have to exhibit a highly deformed conformation. The dendrimer forms a somewhat flattened disklike structure with the hydrophobic groups arranged radial around the dendrimer core, with no hydrophobic groups located on the "top" and "bottom" of the disk. This results in a multidendrimer cylinder with homogeneous core. In this context it is important to note that the dendrimer under investigation, G5 PPI, may not be a large enough dendrimer. It is known that with increasing dendrimer generation the molecular structure changes gradually from starlike to a globular, homogeneous sphere.[1,2] In particular, G5 dendrimers still show flexibility, allowing the molecules to adopt shapes that are far from globular. As Meijer pointed out, such shapes are observed when dendrimers are exposed to "external stimuli", i.e., secondary interactions that force the dendrimers into specific supramolecular arrays.[12] For instance, as mentioned in the Introduction, highly deformed dendrimer structures have been postulated to exist in monolayers, with all the hydrophobic groups of the dendrimer directed toward one side.[20] Further, mesogen-functionalized PPI dendrimers ("dendromesogens") were investigated in the solid state as LC materials[37] with 3,4-bis(decyloxy)benzoyl-modified PPI showing a hexagonal columnar mesophase for G2−G4 but a spheroid structure for G5. The columnar structure should be achieved by piling up three-dimensional segments consisting of a polar core and an apolar shell as the cylinder casing, which is in analogy to the solution structures observed here. Attachment of cyanobiphenyl mesogenic units to PPI dendrimer end groups induced the formation of a smectic A mesophase, in which the dendrimer exhibits a flattened structure.[38] These observations demonstrate the flexibility of the low- to mid-generation dendrimers. In our case the solubilization of salt hydrate represents the driving force for the formation of a supramolecular cylindrical structure consisting of deformed dendrimers. Indeed, we here take advantage of the specific properties of these mid-generation dendrimers being large enough to serve as host and small enough to show the flexibility necessary for assembly into complex structures.

It is further interesting to consider the approximate relative volumes in the dendrimer nanostructures. A G5 PPI dendrimer, having a molecular mass of 7166 g/mol, assuming a density of 1 g/mL, has a volume of 11.9 nm^3. It is then in a collapsed state, i.e., before addition of salt hydrate, a sphere with a radius of 1.4 nm in agreement with the experimental results. As mentioned previously, the amount of gold salt added per dendrimer end groups was in the ratio of 1:1, i.e., 64 molecules of $HAuCl_4 \cdot 3H_2O$. This means 192 water molecules were solubilized per dendrimer molecule, the volume of which is 5.74 nm^3. If the analogy of the hydrophobically modified dendrimers to surfactant micelles is valid, then similar factors may determine the shape of the aggregated structures. The relative volume of the inner hydrophilic part to the outer hydrophobic part, or more accurately the ratio of the surface area of the dendrimer end group to the volume of the inner part, may determine whether spherical or cylindrical structures are formed. Upon solubilization, the volume of the hydrophilic part increases; i.e., the ratio of surface area to volume decreases, and cylindrical structures are favored. On the other hand, however, it has to be noted that the dynamic character of the dendrimer structure and classical micelles is substantially different. To confirm the analogy, different samples with a variation of the relative volume of the inner core would be needed.

As mentioned before, we also prepared samples with different loading ratios. The SANS curves from the saturated and the 1:1 filled sample are the same as expected from the UV−vis results. However, it was not possible to perform SANS measurements on the samples that had less than stoichiometric loading, since the ions became reduced when exposed to the neutron beam for the time period needed to perform the scattering measurement. Likewise, the exposure of the gold-filled samples to laser light as needed for light scattering experiments resulted in reduction of the gold salt. This prevented experiments such as depolarized dynamic light scattering that would be interesting for further investigation of the anisotropic structures. While it is known that gold salts can be easily reduced when exposed to X-ray or neutron beams, the reason for the samples with less gold salt being less stable than the 1:1 loaded is not apparent. An investigation of the influence of the loading ratio on the structure formed should be possible if metal salts of metals less noble than gold are used instead. We will address this issue in future studies.

Use of Dendrimeric Micelles as Confined Reaction Space. Noble metal nanoparticles are currently under discussion for use in areas such as catalysis, solar cell technology, and nonlinear optics. The success in such applications is often dependent on an effective

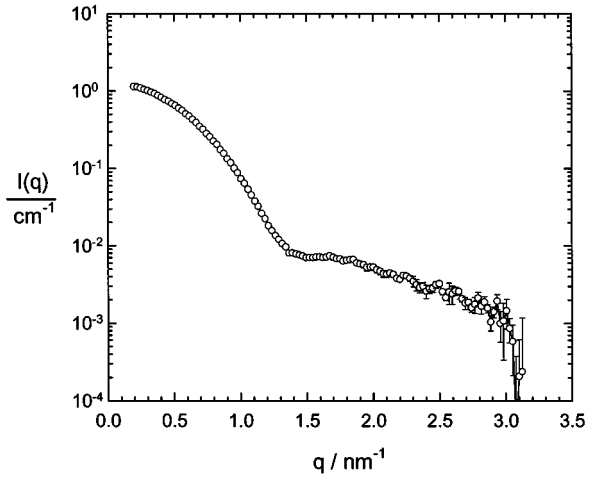

Figure 7. Small-angle neutron scattering curve $I(q)$ for gold−dendrimer hybrid structures. Error bars are the standard deviations of the mean intensity.

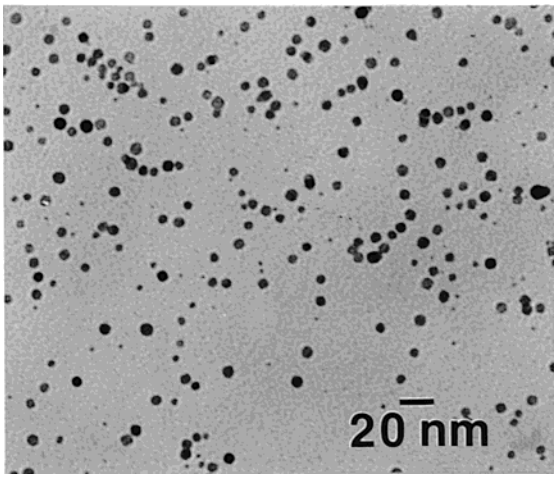

Figure 8. TEM of gold colloids obtained from hydrophobically modified G5 poly(propyleneimine) dendrimers loaded with gold salt after reduction with sodium borohydride.

stabilization of the colloids. In addition, the controlled design of inorganic nanoclusters is of interest. Many studies try to address these tasks by using block copolymer micelles as a nanostructured stabilization environment for the metal particles. The hydrophobically modified dendrimers, however, might provide certain advantages as compared to block copolymer systems. Although the PPI dendrimers are not "unimolecular micelles" when filled, but rather consist of multiple dendrimers, the expression emphasizes the difference from classical surfactant and block copolymer micelles. Because of the highly branched structure of the inner core, the dynamics of the "dendrimeric micelles" should be substantially different from those of conventional micelles. Block copolymer micelles have been claimed to have an advantage over low-molecular-mass surfactant based micelles for their use as confined nanoscale reaction space not only because of the larger size range covered, but in particular due to the different dynamics of the system. The slower exchange of the amphiphilic molecules with higher molecular mass enhances the stability of the nanoreactor. This feature is obviously further improved in a "unimolecular" or "few-molecular" dendrimeric micelle, which should therefore provide an interesting new system to be used as potential nanoreactor. This approach has recently been applied by inner-cross-linking of block copolymer micelles, after the formation of these micelles but prior to their use as a nanoreactor.[39]

With the above motivating factors in mind, we tested the use of dendrimeric "few-molecular" micelles as confined reaction space for the reduction of gold salt. Upon addition of reducing agent, the solution turns brown or red, indicating the formation of colloidal gold. No macroscopic precipitate is observed. The neutron scattering curve for a reduced sample is displayed in Figure 7, and a TEM of gold colloids is shown in Figure 8. As is evident from the shape of the scattering curve and the TEM, reduction of the gold salt yields spherical dendrimer structures and spherical gold particles. This can be caused by the volume change upon reduction due to the density difference of the reduced gold compared to the gold salt hydrate. For all tested reducing methods, the gold colloids are larger than expected when formed within one dendrimer, e.g., 5 nm for the example shown. This is in contrast to the "fixed loading law" observed for dendrimer nanotemplates in homogeneous aqueous solution acting via electrostatic attraction of precursor ions[40] and may be explained by the intermediate linking of dendrimers in the gold-salt-filled structure. The amount of gold salt from multiple dendrimers is then combined to form a single colloidal particle.

All experiments described have been performed at 55 °C, since the fatty acid modified dendrimer is not soluble in toluene at lower temperature. When cooling the gold-colloid-containing solution to room temperature, the gold precipitates with the dendrimer, as can be seen from the color of the precipitate leaving a colorless toluene solution. This observation proves that the gold colloids are indeed connected to the dendrimers. This behavior also allows for an easy separation of the hybrid material from the solvent. The precipitate can be easily redissolved in toluene when reheated to 55 °C.

Although the hydrophobically modified dendrimers form cylindrical structures when filled with gold salt, these cylinders cannot yet be used as template for the formation of cylindrical metal particles. Similarly, the use of cylindrical surfactant or block copolymer micelles or hexagonal morphologies as confined reaction spaces for the formation of noble metal colloids also yields spherical metal particles. However, we consider the large gold particles produced by the reduction as a further confirmation of the intermediate cylindrical connection of multiple dendrimers.

Conclusions

Small-angle neutron scattering and small-angle X-ray scattering have been used as powerful tools for the characterization of solution structures of poly(propyleneimine) dendrimers modified with stearyl end groups in toluene. The structure changes from monomolecular spherical dendrimers to cylindrical multidendrimer assemblies when filled with gold salt hydrate. Upon reduction of the gold salt to metallic gold, spherical gold colloids are formed and the cylindrical structure splits up. The dendrimer−gold hybrid particles may have certain properties that could allow for them to be incorporated into other polymer systems or their use as selective catalysts. While the volume change upon reduction of gold is large, other reactions leading to inorganic materials of lower density could eventually be performed without destruction of the multidendrimer cylinders, allowing for the promotion of the hydropho-

bically modified dendrimers from "nanoscale reactors" to "nanotemplates" for the formation of cylindrical nanocrystals. This is an interesting issue that will be investigated in future studies.

Acknowledgment. We thank Rolf Scherrenberg from DSM for providing us with dendrimers. We thank Yvonne Akpalu for introduction into the SAXS facility and Feng-Ji Yeh and Lizhi Liu for continuous assistance during the SAXS measurements. Ginam Kim and Catheryn Jackson are thanked for help in using the TEM. We thank Heimo Schnablegger, Brent Viers, Paul Butler, Alamgir Karim, and Jack Douglas for helpful discussions. This material is based upon work supported in part by the U.S. Army Research Office under Contract 35109-CH.

References and Notes

(1) Prosa, T. J.; Bauer, B. J.; Amis, E. J.; Tomalia, D. A.; Scherrenberg, R. *J. Polym. Sci.* **1997**, *35*, 2913.
(2) Prosa, T. J.; Bauer, B. J.; Amis, E. J. *Macromolecules* **2001**, *34*, 4897.
(3) Jansen, J. F. G. A.; deBrabander-van den Berg, E. M. M.; Meijer, E. W. *Science* **1994**, *266*, 1226.
(4) Bhyrappa, P.; Young, J. K.; Moore, J. S. *J. Am. Chem. Soc.* **1996**, *118*, 5708.
(5) Bhyrappa, P.; Young, J. K.; Moore, J. S. *J. Mol. Catal. A: Chem.* **1996**, *113*, 109.
(6) Albrecht, M.; Gossage, R. A.; Spek, A. L. *Chem Commun.* **1998**, 9, 1003.
(7) Stevelmans, S.; vanHest, J. C. M.; Jansen, D. A. F. J.; van Boxtel, D. A. F. J.; deBrabander-van den Berg, E. M. M.; Meijer, E. W. *J. Am. Chem. Soc.* **1996**, *118*, 7398.
(8) SayedSweed, Y.; Hedstrand, D. M.; Spindler, R. *J. Mater. Chem.* **1997**, *7*, 1199.
(9) Baars, M. W. P. L.; Froehling, P. E.; Meijer, E. W. *Chem Commun.* **1997**, 1959.
(10) Cooper, A. I.; Londono, J. D.; Wignall, G. *Nature* **1997**, *389*, 368.
(11) Krska, S. W.; Seyferth, D. *J. Am. Chem. Soc.* **1998**, *120*, 3604.
(12) Bosman, A. W.; Janssen, H. M.; Meijer, E. W. *Chem. Rev.* **1999**, *99*, 1665.
(13) Newkome, G. R.; Moorefield, C. N.; Baker, G. R.; Saunders, M. J.; Grossman, S. H. *Angew. Chem., Int. Ed. Engl.* **1991**, *30*, 1178.
(14) Ottiviani, M. F.; Cossu, E.; Turro, N. J. *J. Am. Chem. Soc.* **1995**, *117*, 4387.
(15) Turro, C.; Niu, S. F.; Bossmann, S. H. *J. Phys. Chem.* **1995**, *99*, 5512.
(16) Jansen, J. F. G. A.; Meijer, E. W.; deBrabander-van den Berg, E. M. M. *Macromol. Symp.* **1996**, *102*, 27.
(17) Chow, H. F.; Chan, I. Y. K.; Chan, D. T. W. *Chem. Eur. J.* **1996**, *2*, 1085.
(18) Pollak, K. W.; Leon, J. W.; Frechet, J. M. J. *Chem. Mater.* **1998**, *10*, 30.
(19) Vassilev, K.; Ford, W. T. *J. Polym. Sci., Part A* **1999**, *37*, 2727.
(20) Schenning, A. P. H. J.; Elissen-Roman, C.; Weener, J. W.; Baars, M. W. P. L.; vander Gast, S. J.; Meijer, E. W. *J. Am. Chem. Soc.* **1998**, *120*, 8199.
(21) Weener, J. W.; Meijer, E. W. *Adv. Mater.* **2000**, *12*, 741.
(22) deBrabander-van den Berg, E. M. M.; Meijer, E. W. *Angew. Chem.* **1993**, *105*, 1370.
(23) Certain commercial materials and equipment are identified in this article in order to specify adequately the experimental procedure. In no case does such identification imply recommendation by the National Institute of Standards and Technology, nor does it imply that the material or equipment identified is necessarily the best available for this purpose.
(24) Hammouda, B.; Krueger; S.; Glinka, C. *J. Res. Natl. Inst. Stand. Technol.* **1993**, *98*, 31.
(25) Hsiau, B. S.; Chu, B.; Yeh, F. *NSLS Newsletter* **1997**, July1.
(26) Glatter, O. *Acta Phys. Austriaca* **1977**,*47*, 83
(27) Glatter, O. *J. Appl. Crystallogr.* **1977**, *10*, 415.
(28) Glatter, O. *J. Appl. Crystallogr.* **1980**, *13*, 7 and 577.
(29) Glatter, O. *J. Appl. Crystallogr.* **1981**, *14*, 101.
(30) Glatter, O.; Hainisch, B. *J. Appl. Crystallogr.* **1984**, *17*, 435.
(31) Glatter, O. *J. Appl. Crystallogr.* **1988**, *21*, 886.
(32) Ramzi, A.; Bauer, B. J.; Scherrenberg, R.; Froehling, P.; Joosten, J.; Amis, E. J. *Macromolecules* **1999**, *32*, 4983.
(33) Bauer, B. J.; Amis, E. J. NISTIR 6353, 1999, and unpublished results.
(34) Topp, A.; Bauer, B. J.; Prosa, T. J.; Scherrenberg, R.; Amis, E. J. *Macromolecules* **1999**, *23*, 8923.
(35) Berlepsch, H.; Mittelbach, R.; Hoinkis, E.; Schnablegger, H. *Langmuir* **1997**, *13*, 6032.
(36) Maurer, N.; Cantu, L.; Glatter, O. *Chem. Phys. Lipids* **1995**, *78*, 54.
(37) Cameron, J. H.; Facher, A.; Lattermann, G.; Diele, S. *Adv. Mater.* **1997**, *9*, 398.
(38) Baars, M. W. P. L.; Söntgens, S. H. M.; Fischer, H. M.; Peerlings, H. W. I.; Meijer, E. W. *Chem. Eur. J.* **1998**, *4*, 2456.
(39) Förster, S.; Wenz, E., personal communication.
(40) Gröhn, F.; Bauer, B. J.; Akpalu, Y. A.; Jackson, C. L.; Amis, E. J. *Macromolecules* **2000**, *33*, 6042.

MA0017384